RSC Advances

ROYAL SOCIETY OF CHEMISTRY

www.rsc.org/advances

RSC Advances

ARTICLE

Flux Growth of Patterned $LiCoO_2$ Crystal Arrays Directly on Pt Substrate in Molten $LiNO_3$

Received 00th January 20xx,
Accepted 00th January 20xx

DOI: 10.1039/x0xx00000x

www.rsc.org/

T. Yoda,[a,b] N. Zettsu,[a,c,d] H. Onodera,[a] Y. Mizuno,[a,d] H. Kondo,[b] and K. Teshima[a,c,d,*]

We demonstrate a new way to prepare hollow-structured $LiCoO_2$ crystals directly on a Pt substrate for the first time through a combination of semi-additive electrodeposition of a Co core and subsequent flux growth in molten $LiNO_3$. The reaction process was characterized by time-dependent X-ray diffraction and scanning electron microscopy. The vertically oriented crystals having a platelet shape grew densely on the Co dot surface. The crystal growth was driven by supersaturation in the same manner as the flux growth. Significant slower oxidation of the Co core and rapid lithiation of Co_3O_4 lead to pore formation, which suggests that slow oxygen diffusion in the Co core is rate limiting. Galvanostatic tests revealed that the $LiCoO_2$ crystal array exhibited typical capacity-voltage profiles with no heavy capacity loss during the first three cycles without any additives.

Introduction

Flux growth is one of the most versatile ways to obtain idiomorphic crystals at low temperatures without any thermal strain or defects from high-temperature solutions.[1-3] Thus, it has many advantages over other techniques of functional material synthesis. For instance, flux growth methods provide well-faceted single crystals, which improve lithium ion secondary battery (LIB) performances. The flux of LiCl, NaCl, KCl, NaCl-KCl, and LiCl-KCl enables the growth of layered $LiCoO_2$[4,5], $Li(Ni_{0.8}Mn_{0.1}Co_{0.1})O_2$[6], spinel $LiMn_2O_4$[7,8], $Li_4Ti_5O_{12}$[9,10], and olivine $LiFePO_4$[11-13] crystals, which show significantly enhanced electrochemical performances with high capacity, excellent cycle stability, and good rate capability. In addition, such nicely faceted crystals exhibit face-selective properties such as face-selective tolerance towards the loss of electrolyte-soluble transition metal ions in the crystals.[14]

Flux growth techniques provide several aspects of desired crystal growth by adjustment or optimization of growth conditions. For instance, the flux selected and the additives or mineralizers used, such as OH^-, F^-, Cl^-, affect crystal nucleation and growth, so they affect the crystal size, shape, and habit through the dissolution of the reagents by complex formation in solution. This increases the metastable region where supersaturation can occur, and alternating the viscosity of the hot solutions.[1,2]

Very recently, we extended the flux growth concept to a coating technique for fabricating a polycrystal film deposited directly on substrates.[10,11,15] High-quality crystals were grown using a paste composed of the solutes and flux for the growth, which were coated onto the substrate prior to heating. The substrate surface was fully covered with well-defined faceted single crystals. Cross-sectional transmission electron microscopy (TEM) observation along with EDS and SAED analysis revealed that at the interface, strong bonding exits on the atomic level between the crystals and the substrate with no impurity phase. Time-dependent X-ray diffraction (XRD) and scanning electron microscopy (SEM) suggested that the crystal growth mechanism was analogous to flux growth driven by supersaturation. The initial heterogeneous nucleation and subsequent growth in a homogeneous hot solution resulted in the formation of the crystal layer on the substrate. We called this new coating methodology *flux coating*. The $LiCoO_2$, $Li_4Ti_5O_{12}$ polycrystal films showed a large capacity close to the theoretical values with no assistance from any additives such as carbon black and polyvinylidene fluoride (PVDF) under moderate C rate conditions.[10,15] This indicated that Li^+ ions and electrons were efficiently transferred in the electrode and interfaces during the intercalation and deintercalation reaction. Thus, we believe such additive-free electrodes potentially enhance the specific energy density per electrode volume.

For expanding the application of additive-free electrodes produced by flux coating, we propose a new way to prepare desirable additive-free electrodes directly on a substrate using a combination of electrodeposition of transition metals and flux coating. This is advantageous because electrodeposition is a powerful means of mass production of thin metal films at a low cost. Furthermore, micrometer-scale architectures can be

[a] Department of Environmental Science & Technology, Shinshu University, 4-17-1 Wakasato, Nagano 380-8553, Japan. E-mail: teshima@shinshu-u.ac.jp
[b] SHINKO ELECTRIC INDUSTRIES CO. LTD, 80 Oshimada-machi, Nagano 381-2287, Japan.
[c] Center for Energy and Environmental Science, Shinshu University, 4-17-1 Wakasato, Nagano 380-8553, Japan.
[d] JST-CREST

Electronic Supplementary Information (ESI) available: [details of any supplementary information available should be included here]. See DOI: 10.1039/x0xx00000x

formed via combined photolithography and a lift-off technique with electrodeposition. This process is called semi-additive electrodeposition. Macroscopic architectures of electrodes in LIBs increase the reactive surface area as well as accelerate the Li-ion transfer at the electrolyte interface, leading to high energy transfer.[16-18] For instance, Pikul et al.[18] demonstrated continuous microporous electrodes using a combination of colloidal self-assembly of polystyrene nanospheres as the template and electrodeposition of active materials; the resulting electrodes exhibited a micro-architecture and achieved high rate capabilities. However, to the best of our knowledge, there are no previous reports on electrodeposited Co with the fine patterns obtained by using semi-additive electrodeposition.

In this study, we demonstrate the fabrication of spatially designed $LiCoO_2$ crystal assemblies and control their periodicity through a combination of semi-additive electroplating of metallic Co and flux growth of $LiCoO_2$ crystals in molten $LiNO_3$, which realizes uniform, low-cost, and large-scale production of designed LIBs electrodes. We characterized the reaction process using time-dependent XRD and SEM. We also characterized their primitive electrochemical properties for use as cathodes for LIBs using galvanostatic tests.

Experimental Section

A mixed aqueous solution containing 350 g/L of cobalt sulfate ($CoSO_4 \cdot H_2O$ 350 g/L), 30 g/L of cobalt chloride ($CoCl_2 \cdot 6H_2O$), 30 g/L of boric acid, and malonic acid as an organic acid having carboxyl groups was used for Co plating. The pH and temperature of the mixed solution were maintained at 4.0 and 50 °C, respectively, during the plating. Ammonia water and an aqueous solution of sulfuric acid were used as pH adjusters. A photolithographic technique followed by a lift-off process was applied to prepare the templates for the fabrication of the spatially designed Co microstructures. A dry film developed by Hitachi Chemical Corporation was used as a photoresist. The photoresist film was used to laminate a clean Pt substrate. The thickness of the photoresist was ~15 μm. After irradiation with UV light, the unreacted resist film was developed using an aqueous solution of sodium carbonate. The plating process was progressed in two steps by tuning the current density first to 6.0 A/dm^2 for 1 min and then to 2.0 A/dm^2. The thicknesses of the Co layers were controlled to be 7 μm. Finally, the dry film was removed carefully by using *n*-methyl pyrolidone. Spatially patterned electrodeposited Co cores were converted to $LiCoO_2$ crystals in molten $LiNO_3$ at 500 °C. Platinum substrates with 0.1 mm thickness were used in this study as a priority in validating the evidence of our demonstration. Lithium nitrate was used as both a Li source and a flux for the growth. The concentration of the aqueous $LiNO_3$ solution was 30 wt%. Ten milliliters of the aqueous $LiNO_3$ solution was spread onto the Co layer with dimensions of 10 × 10 mm by drop casting. The corresponding solute concentration was 2.65 wt%. The substrate was heated to 500 °C at a rate of 1000 °C/h in an electric furnace. After maintain the temperature for 10 h, the crucible was cooled to 100 °C at rate of 200 °C/h. The heated substrates were then naturally cooled to room temperature in the furnace. Finally, the substrates were immersed in warm water at 80°C for 30 min to remove the remaining flux. The washed substrate was dried at 100 °C under air. The morphology and average size of the grown $LiCoO_2$ crystals were characterized using field-emission scanning electron microscopy (FE-SEM, JEOL, JSM-7600F). The acceleration voltage was of 15 kV. The samples for the cross-sectional SEM observation were prepared by focused ion beam milling (FIB, JEOL, JIB-4601F) with a Ga-ion source. The FIB milling was performed at 30 kV. A tungsten layer was deposited on the sample surfaces as a protection layer prior to milling. The phases and structures of the crystals were identified using XRD analysis with Cu kα radiation. The X-ray diffractometer (RIGAKU, MiniflexII) was operated at 30 kV and 20 mA, with 2θ = 10–80°. The charge–discharge characteristics of the $LiCoO_2$ crystal layer as an additive-free cathode were studied using a coin-type cell (R2032 type). A galvanostatic charge–discharge test was conducted using a battery tester (HOKUTO DENKO, HJ1001SD8) with a voltage window of 2.5–4.2 at setting current rate. The $LiCoO_2$ crystals on the Pt substrates were annealed at 700 °C for 1 h under air to promote crystallization prior to cell assembly. A mixed solution of ethylene carbonate and dimethyl carbonate containing 1 M of $LiPF_6$ was used as an electrolyte. Li metal foil was used as an anode. A polypropylene separator (Celgard separator #2400) was used for the suppression of direct contact of each electrode. The coin-type LIBs were assembled in an Ar-filled glove box (MIWA MFG Co. Ltd.) with a controlled atmosphere containing less than 1 ppm of H_2O and O_2.

Results and Discussion

In general, Co can be electrodeposited from the Co^{2+}-containing solutions stabilized with sulfate chloride, ammonium sulfamate, and fluoborate.[19-23] As a result, Co plating films hardly adhere to electrodes owing to the high interface stress. Therefore, the Ni plating process was commonly employed for strain release before Co deposition was initiated. The thin soft Ni layer worked as a buffer. From the viewpoint of material synthesis, however, the external metal species becomes a potential source of impurity or sub-phase formation. Thus, we demonstrated two-step Co electrodeposition under different current densities, without employing the Ni layer.

Typical SEM images of the Co microstructures are shown in Figures 1(a) and (b). Ultra-fine Co dot matrices arranged in a 4-fold symmetry were uniformly formed with 10 × 10 cm dimensions. Figure 2 (a), (e) show the changes in XRD profiles of the microstructured Co electrodeposits after heating in molten $LiNO_3$ flux at 500 °C for 50 h. All diffraction lines in Figure 2 (e) can be assigned as per the International Centre for Diffraction Data (ICDD) for $LiCoO_2$ (PDF 75-0532), which belongs to an *R*-3*m* space group and the Pt substrate. The lattice parameters were determined to be a = 2.819 and c = 14.101 Å. These values closely agree with previous data.[4, 24-27] $LiNO_3$ flux decreased the reaction temperature

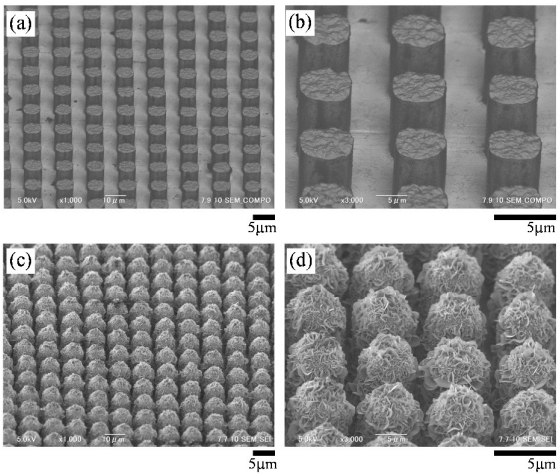

Figure 1. Changes in the 45°-tilted FE-SEM images of the Co dot arrays directly deposited on the Pt substrate: (a, b) as prepared Co dot with average diameter of 7 μm (c, d) after heating at 500°C for 50h in a molten $LiNO_3$.

drastically to 500 °C, lower than that of solid-state-reaction processes. Notably, the relative intensities of the diffraction lines at 2θ = 18.93/45.26, assigned to 003_{LiCoO2} /104_{LiCoO2}, were less than that as per the ICCD data, suggesting that the $LiCoO_2$ crystals were dominantly covered with 104_{LiCoO2} planes. As shown in Figure 1 (c) and (d), SEM observation showed the Co dots were uniformly transformed into hemispherical dots that maintained their original periodicity. The numerous small crystals with platelet shapes were formed densely in the hemispherical dots. It is appeared that all individual crystals were oriented perpendicularly toward the surface. The platelet shape of the $LiCoO_2$ crystal is known to be the result of a thermodynamically favored state produced under an oxidative atmosphere.[4, 5, 24-27] The wide flat plate of the crystal can be assigned to the *c*-plane, and their sharp and asymmetrical side faces are surrounded by *a*, *b* faces.

To gain insight into the reaction mechanism responsible for $LiCoO_2$ phase formation, time-dependent *ex situ* XRD measurements and SEM observation were carried out. Figure 2 (a)-(e) show the changes in the XRD profiles of the Co dot matrix having 7 μm diameter as a function of reaction time at 500 °C. The $LiCoO_2$ phase was formed as the primary phase after 1 h despite the coexistence of metallic Co, $Li_{0.6}Co_{0.94}O$ and Co_3O_4. The diffraction lines attributed to Co metal completely disappeared after 10 h. Instead, both the diffraction intensity of $Li_{0.6}Co_{0.94}O$ and Co_3O_4 increased. Further increase in the reaction time to 50 h resulted in the formation of $LiCoO_2$ as a single component. The formation of the CoO phase as an intermediate[5] was not detected by *ex-situ* XRD measurement during the whole reaction process. This suggests that $LiNO_3$ oxidizes Co to be Co_3O_4 with an assistance of Co as catalysts for the decomposition of $LiNO_3$, and Li^+ and NO_2 were released in hot melt at 500°C, as following plausible reaction scheme:

$$4\ LiNO_3 + Co \rightarrow 4\ NO_2 + Co_3O_4 + 4Li^+$$

Then $LiCoO_2$ was immediately formed via lithiation of Co_3O_4. Implying that the kinetics in the $LiCoO_2$ formation in molten $LiNO_3$ might be limited by the oxidation of Co to Co_3O_4 owing to slow O_2 diffusion into bulk Co.

Figures 3 and 4 show the changes in surface and cross-sectional SEM images of 7 μm-sized Co dots during the growth, respectively. All Co deposits surface in Figure 4 was covered with a tungsten layer prior to FIB milling for stabilization. The as-deposited Co dots

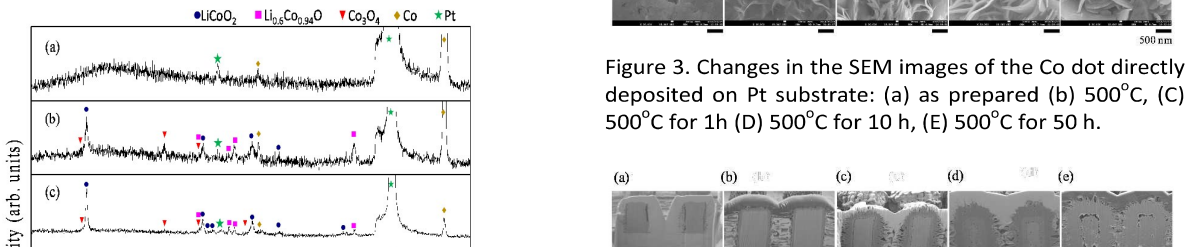

Figure 2. Changes in the XRD profiles of the Co dot directly deposited on Pt substrate: (a) as prepared (b) 500°C, (C) 500°C for 1h (D) 500°C for 10 h, (E) 500°C for 50 h.

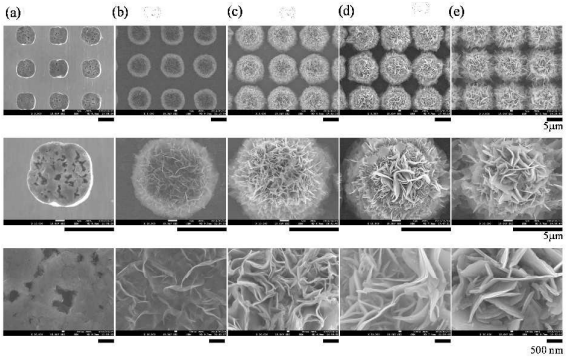

Figure 3. Changes in the SEM images of the Co dot directly deposited on Pt substrate: (a) as prepared (b) 500°C, (C) 500°C for 1h (D) 500°C for 10 h, (E) 500°C for 50 h.

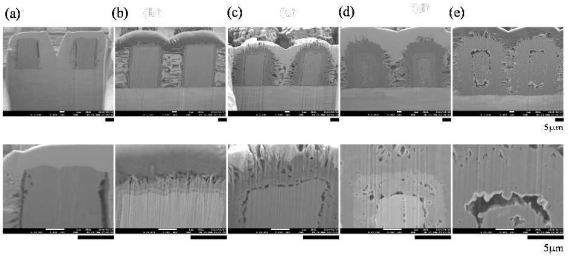

Figure 4. Changes in the cross-sectional SEM images of the Co dot directly deposited on Pt substrate: (a) as prepared (b) 500°C, (C) 500°C for 1h (D) 500°C for 10 h, (E) 500°C for 50 h.

transformed to cylindrical shapes with an aspect ratio of ca. 1.5. Even after heating for 1 h, numerous crystals with platelet shapes spread over the Co surface. Corresponding cross-sectional SEM images clearly show that the individual $LiCoO_2$ crystals grew radially out from the Co dot surface. The length and width of an individual crystal is approximately 1 µm and ~200 nm, respectively. Notably, three different contrasts were observed in the core. According to corresponding SEM-EDS mapping (Figure S1), a dense shell layer of $LiCoO_2$ and/or $Li_{0.6}Co_{0.94}O$ as well as a core of Co and/or Co_3O_4 were considered to form in the hemispherical assemblies. Furthermore, a nanometer-scale space was formed along the core/shell interface, as shown in Figure 4b. Both the platelet crystal growth and dense $LiCoO_2$ shell thickness further increased with the reaction time (Figure 4c-e). All these phenomena implied $LiCoO_2$ formation via Co_3O_4 strongly associated with the void formation driven by the Kirkendall effect,[27-30] which results from the difference between solid-state diffusion rates of the core materials and the rate of O_2 diffusion through the shell at the elevated temperatures during oxidation.[31] We consider that slow O_2 diffusion limited $LiCoO_2$ formation and the low solubility of $LiCoO_2$ in molten $LiNO_3$ at the relatively low temperature of 500°C might create steep gradient of supersaturation toward the surface of Co dots. Such a steep gradient of supersaturation tends to promote the anisotropic crystal growth of $LiCoO_2$ perpendicularly to the Co dot surface driven by kinetic control.[9]

The plausible formation mechanism based on the above mentioned data is schematically illustrated in Figure 5. The $LiCoO_2$ phase formation was limited kinetically by oxidation of Co to Co_3O_4 due to slow O_2 diffusion in bulk Co. The $LiCoO_2$ layer were formed immediately from the Co dot surface through the oxidation of Co with resolved O_2 and following solid-solution reaction of solid Co_3O_4 with liquid-phase $LiNO_3$. Because the solubility of $LiCoO_2$ in a molten $LiNO_3$ is low, a small fragment of exposed top part of the $LiCoO_2$ layer was dissolved in the molten $LiNO_3$, leading increased concentration of liquid-phase $LiCoO_2$ around the solid/liquid interface. Simultaneously, the movement of the interface between the diffusion couples of Co_3O_4 and Co in the core occurred, as the result of the different diffusion rates of Co and O_2 at the elevated temperature. Directional material flows resulted from coupled reaction-diffusion phenomena at the solid Co/liquid $LiNO_3$ interface considered to lead to void formation. These voids might be explained by outward transport of fast-moving Co through the top Co_3O_4 oxide layer and a balancing inward flow of vacancies to the vicinity of the Co_3O_4 interface. We believe that these two kinetically

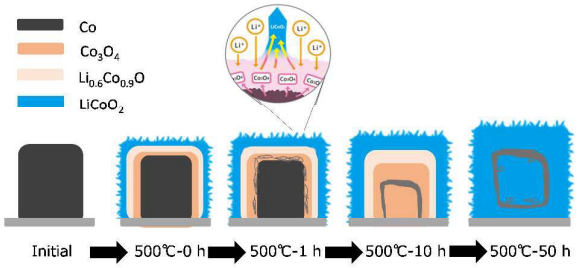

Figure 5. Schematic illustration of the plausible mechanism of the $LiCoO_2$ dot array formation.

different reactions created the situation of anisotropic growth of $LiCoO_2$ perpendicularly to the Co dot surface, driven by a kinetically controlled mode. This growth mechanism was strongly similar to that of the growth of the oriented $Na_2Ti_3O_7$ whiskers from Ti mesh surface using a NaCl flux.[34] Once platelet-shaped $LiCoO_2$ crystals were grown from the Co dot surface, the following growth reaction promoted preferential attachment growth along the <001> directions surrounded by {101} and {104} faces of rhombohedral phased $LiCoO_2$ by kinetically controlled growth.[15, 35]

Finally, the primitive electrochemical properties of 7 µm-sized $LiCoO_2$ dot arrays as an additive-free LIB-cathode obtained after 10 h of growth was studied. The substrate was heated at 700 °C for 1h under air to promote crystallization. The *a*, *b* faces in the $LiCoO_2$ dot arrays became wide through the contribution of atomic diffusion on the $LiCoO_2$ crystals into the adjacent $LiCoO_2$ crystals at high temperature annealing.[15] In addition, the post heating treatment caused a growth of the nanospace formed within the $LiCoO_2$ dot. (Figure S2) Galvanostatic cycling measurements were conducted using R2032 coin-type cells. No additives for the enhancement of their electron conductivity were used for the studies. Figure 6 shows the first three cycles of capacity-voltage profiles in the potential range of 2.0-4.2 V vs. Li/Li^+, measured at a current density of 50 µA·cm^{-2}, corresponding to 0.1C. One C rate indicates the current required to obtain a full charge in 1 h. Excellent reversibility with a high coulomb efficiency was observed after the second cycle even with no additives, although some irreversible capacity was observed in the first cycle. Owing to the formation of a solid-electrolyte interface (SEI) during the first LIB charging cycle, that the coulombic efficiency seems to be lower; this agrees with trends observed for commercial $LiCoO_2$-based cathodes.[24-27] In fact, during the second and subsequent cycles, the coulombic efficiency was recovered to ca. 98%. Therefore, the primitive galvanostatic test demonstrated here revealed that the hollow-structured $LiCoO_2$ crystal array exhibited typical capacity-voltage profiles without any additives. This indicated that electrons were efficiently transferred at the electrode/current collector interface during the intercalation and deintercalation reaction. Meaning that the interfaces provide seamless charge transportation pathways. We further studied the

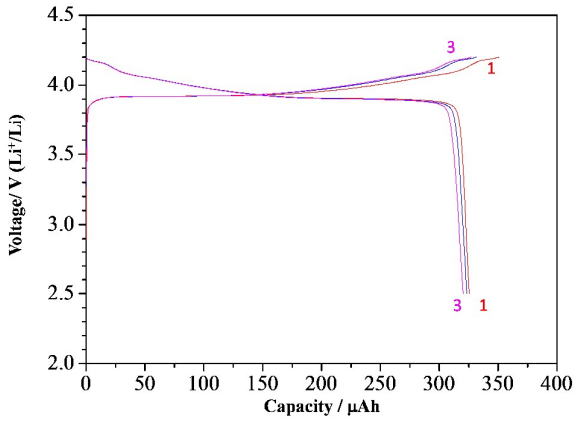

Figure 6. First 3 charge and discharge curves of the 7 µm-$LiCoO_2$ dot array electrode.

effects of the $LiCoO_2$ dot size on the capacity by comparing the Co dot diameter of 7 μm and 9 μm with almost same coating weight the $LiCoO_2$ dot array, shown in Figure S3. The current capacity was noticeably dropped by the increase of the dot size. Thus, we believe such additive-free electrodes with high surface area potentially enhance the specific energy density per electrode volume.

Conclusions

Flux growth of $LiCoO_2$ crystal arrays from the semi-additive-electrodeposited Co dots in molten $LiNO_3$ opens up a new route for the fabrication of microscopically designed $LiCoO_2$ electrodes, which potentially offers significant flexibility in material design and substantially lower cost. It can therefore be responsible for low-cost production of diverse-material LIBs. Time-dependent SEM and XRD studies suggested that the conversion process kinetics involve different reactions, including low $LiCoO_2$ phase formation leading to hollow structures based on the Kirkendall effect and rapid growth of $LiCoO_2$ crystals promoting anisotropic growth. Galvanostatic tests revealed that the hollow-structured $LiCoO_2$ crystal array exhibited typical capacity-voltage profiles with no heavy capacity loss during the first three cycles without any additives. Because the additive-free electrode of $LiCoO_2$ demonstrated here showed similar electrochemical performances of commercially available $LiCoO_2$ based electrodes under the condition of low current density, desirable battery micro-architectures prepared by the combination of semi-additive electrodeposition with flux coating will potentially realize a high energy density and high power density simultaneously owing to additive-free electrodes and the high reactive surface area, respectively. Evaluation of electrochemical characteristics of the additive-free electrodes under a high current density is in progress, and we hope to publish the results in the near feature.

Acknowledgements

This work was partially supported by JSPS Grants-in-Aid for Scientific Research (A) (KAKENHI) Grand Number 25249089.

Notes and references

‡ Footnotes relating to the main text should appear here. These might include comments relevant to but not central to the matter under discussion, limited experimental and spectral data, and crystallographic data.

1 D E. Bugaris, H-C. zur Loye, Angew. Chem. Inter. Ed. 2012, **51**, 3780.
2 D. Elwell, H. J. Scheel, Crystal Growth from High-Temperature Solutions, Academic Press, New York, 1975.
3 S. Oishi, K. Teshima and H. Kondo, J. Am. Chem. Soc., 2004, **126**, 4768.
4 K. Teshima, S. Lee, Y. Mizuno, H. Inagaki, M. Hozumi, K. Kohama, K. Yubuta, T. Shishido and S. Oishi, Cryst. Growth Des., 2010, **10**, 4471.
5 N. Zettsu, K. Nishikawa, K. Yubuta, K. Sakurai, Y. Yamamoto, Y. Mizuno, S. Oishi, K. Teshima, J. Mater. Chem. A, 2015, **3**, 17016.
6 Y. Kim, ACS Appl. Mater. Interfaces 2012, **4**, 2329.
7 Y. Mizuno, N. Zettsu, H. Inagaki, S. Komine, K. Kami, K. Yubuta, H. Wagata, S. Oishi, K. Teshima, CrystEngComm., 2014, **16**, 1157.
8 X. J. Yang, W. P. Tang, H. Kanoh and K. Ooi, J. Mater. Chem., 1999, **9**, 2683.
9 K. Teshima, H. Inagaki, S. Tanaka, K. Yubuta, M. Hozumi, K. Kohama, T. Shishido and S. Oishi, Cryst. Growth Des., 2011, **11**, 4401.
10 N. Zettsu, Y. Mizuno, H. Kojima, K. Yubuta, T. Sakaguchi, T. Saito, H. Wagata, S. Oishi, and K. Teshima, Cryst. Growth Des., 2014, **14**, 5634.
11 T. Yamada, N. Zettsu, N. Handa, S. Oishi, K. Teshima, Cryst. Growth Des. 2015, **15**, 3922.
12 Y. Janssen Y, D. Santhanagopalan D. Qian, M. Chi, X. Wang, C. Hoffmann, Y. S. Meng, P. G. Khalifah, Chem. Mater., 2013, **25**, 4574.
13 J. Li, W. Yao, S. Martin, D. Vaknin, Solid State Ionics, 2008, **179**, 2016.
14 M. Hirayama, H. Ido, K. Kim, W. Cho, K. Tamura, J. I. Mizuki and R. Kanno, J. Am. Chem. Soc., 2010, **132**, 15268.
15 Y. Mizuno, N. Zettsu, K. Yubuta, T. Sakaguchi, T. Saito, H. Wagata, S. Oishi, K. Teshima, Cryst. Growth Des. 2014, **14**, 1882.
16 C. Liu, Z. Yu, D. Neff, A. Zhamu, B. Z. Jang, Nano Lett., 2010, **10**, 4863; Y. Zhu, S. Murali, M. D. Stoller, K. J. Ganesh, W. Cai, P. J. Ferreira, A. Pirkle, R. M. Wallace, K. A. Cychosz, M. Thommes, D. S. Eric, A. Stach, R. S. Ruoff, Science, 2011, **332**, 1537.
17 D. Pech, M. Brunet, H. Durou, P. Huang, V. Mochalin, Y. Gogotsi, P.-L. Taberna, P. Simon, Nature Nanotech., 2010, **5**, 651.
18 J. H. Pikul, H. G. Zhang, J. Cho, P. V. Braun, W. P. King, Nature Comm., 2013, **4**, 1732.
19 F.E. Rasmussen, J.T. Ravnkilde, P.T. Tang, O. Hansen and S. Bouwstra, Sens. Actuators A, 2001, **92**, 242.
20 A. A. Karimpoor, U. Erb, K. T. Aust, G. Palumbo, Scripta Mater., 2003, **49**, 651.
21 S. H. Kim, K. T. Aust, U. Erb, F. Gonzalez and G. Palumbo, Scripta Mater., 2003, **48**, 1379.
22 X. Deng, P. Wei, M.R. Bateni and A. Petric, J. Power Sources, 2006, **160**, 1225.
23 V. Kublanovsky, O. Bersirova, Y. Yapontseva, H. Cesiulis and E.P. Murphy, Prot. Met., 2009, **45**, 588.
24 C.-H. Han, Y.-S. Hong, Y.-S. Park, K. Kim, J. Power Sources, 2001, **92**, 95.
25 H. Wang, Y. I. Jang, B. Huang, D. R. Sadoway, Y. M. Chiang, J. Electrochem. Soc. 1999, **146**, 473–480.
26 J. N. Reimers,, J. R. Dahn, J. Electrochem. Soc. 1992, **139**, 2091.
27 J. Xie, N. Imanishi, T. Zhang, A. Hirano, Y. Takeda, O. Yamamoto, J. Power Sources 2009, 189, 365.
28 A. D. Smigelskas, E. O. Kirkendall, Trans. AIME, 1947, **171**, 130.
29 C. E. Birchenall, J. Electrochem. Soc., 1956, **103**, 619.
30 J. C. Colson, M. Lambertin, P. Barret, in Proc. 7th Int. Symp. Reactivity of Solids, J. S. Anderson, F. S. Stone, M. W. Roberts, Eds. (Chapman & Hall, London, 1972), pp. 283–293.
31 Y. Yin, R. M. Rioux, C. K. Erdonmez, S. Hughes, G. A. Somorjai, A. P. Alivisatos, Science, 2004, **30**, 711; S. Mrowec, M. Danlelewski, A. Wojtowicz, J. Mater. Sci., 1998, **33**, 2617.
32 Justin G. Railsback, Aaron C. Johnston-Peck, Junwei Wang, and Joseph B. Tracy, ACS Nano, 2010, **4**, 1913.
33 Joseph B. Tracy, Dirk N. Weiss, Dmitry P. Dinega, and Moungi G. Bawendi, Phys. Rev. B, 2005, **72**, 064404.

34 K. Teshima, S. H. Lee, S. Murakoshi, S. Suzuki, M. Kiyohara, K. Yubuta, T. Shishido, M. Endo, S. Oishi, Cryst. Growth. Des., **10**, 2010, 2533.
35 K. Takahashi, S. J. Limmer, Y. Wang, G. Z. Cao, Jpn. J. Appl. Phys. 2005, **44**, 662.